Biophysical *Journal*
Article

Biophysical Society

Going with the Flow: Water Flux and Cell Shape during Cytokinesis

Yizeng Li,[1] Lijuan He,[2] Nicolas A. P. Gonzalez,[2] Jenna Graham,[2] Charles Wolgemuth,[5] Denis Wirtz,[2,4] and Sean X. Sun[1,3,4,*]

[1]Departments of Mechanical Engineering, [2]Chemical and Biomolecular Engineering, [3]Biomedical Engineering, and [4]Institute of NanoBioTechnology, Johns Hopkins University, Baltimore, Maryland; and [5]Department of Physics, University of Arizona, Tucson, Arizona

ABSTRACT Cell shape changes during cytokinesis in eukaryotic cells have been attributed to contractile forces from the actomyosin ring and the actomyosin cortex. Here we propose an additional mechanism where active pumping of ions and water at the cell poles and the division furrow can also achieve the same type of shape change during cytokinesis without myosin contraction. We develop a general mathematical model to examine shape changes in a permeable object subject to boundary fluxes. We find that hydrodynamic flows in the cytoplasm and the relative drag between the cytoskeleton network phase and the water phase also play a role in determining the cell shape during cytokinesis. Forces from the actomyosin contractile ring and cortex do contribute to the cell shape, and can work together with water permeation to facilitate cytokinesis. To influence water flow, we osmotically shock the cell during cell division, and find that the cell can actively adapt to osmotic changes and complete division. Depolymerizing the actin cytoskeleton during cytokinesis also does not affect the contraction speed. We also explore the role of membrane ion channels and pumps in setting up the spatially varying water flux.

INTRODUCTION

Flow of water across the cell membrane, made possible by intrinsic permeability of the membrane and the presence of aquaporins, is vital in essential processes such as kidney water reabsorption (1), cell volume regulation (2), cell cytoplasmic ionic balance (3), and cell motility (4). Water flow across the membrane is driven by both hydrostatic and osmotic pressure differences (5). Fig. 1 *a* illustrates elements of water permeation driven by osmotic gradients. When the membrane is flexible and is not mechanically constrained, it is displaced by water and moves in the opposite direction of water flux. This membrane movement, which changes the overall cell shape, can occur locally or globally, depending on the spatial arrangement of osmotic gradients. Here we explore the role of water flux during cytokinesis, which is another essential cell process that requires a large cell shape change. Using modeling and supporting experiments, we show that in addition to cytoskeleton-based mechanisms, spatially controlled water flux generated by the cell can also achieve the same cell shape change during cytokinesis.

Many mechanical processes in cells have been attributed to actin and the microtubule cytoskeleton. For instance, cell movement on substrates requires actin cytoskeleton. However, there is now an increasing appreciation of the role of hydrodynamics in cell mechanics (6–11). It was found that some cells in 1D narrow channels can move in an actomyosin-independent manner (4,12). Similar actin-independent migration was observed in glioblastoma (13). Water flux was found to increase cell speed in actin-dependent motility (14). Water flux-associated cell and nuclear volume change are also connected with cell-matrix adhesion (15). As the role of hydrodynamics in cell function becomes clearer, there is a need to understand how water flow and cytoskeletal network dynamics are coupled, and to develop a general modeling framework to treat such problems.

Experiments have shown that an actomyosin contractile ring has been identified as the force generator in eukaryotic cytokinesis (16,17). For example, inhibition of myosin II in HeLa cells and normal rat kidney epithelial cells arrests furrow ingression (18,19). However, there are exceptions. *Dictyostelium discoideum*, when anchored to the substrate, can form a division furrow while myosin II is abolished (20). The ciliate *Tetrahymena pyriformis* is still able to form a division furrow when actin polymerization is inhibited (21). These results suggest that cells potentially can employ multiple force-generating mechanisms available to ensure successful division. For example, exocytosis may participate in furrow ingression and contribute to the increased area of

Submitted April 20, 2017, and accepted for publication September 26, 2017.
*Correspondence: ssun@jhu.edu
Editor: David Odde.
https://doi.org/10.1016/j.bpj.2017.09.026

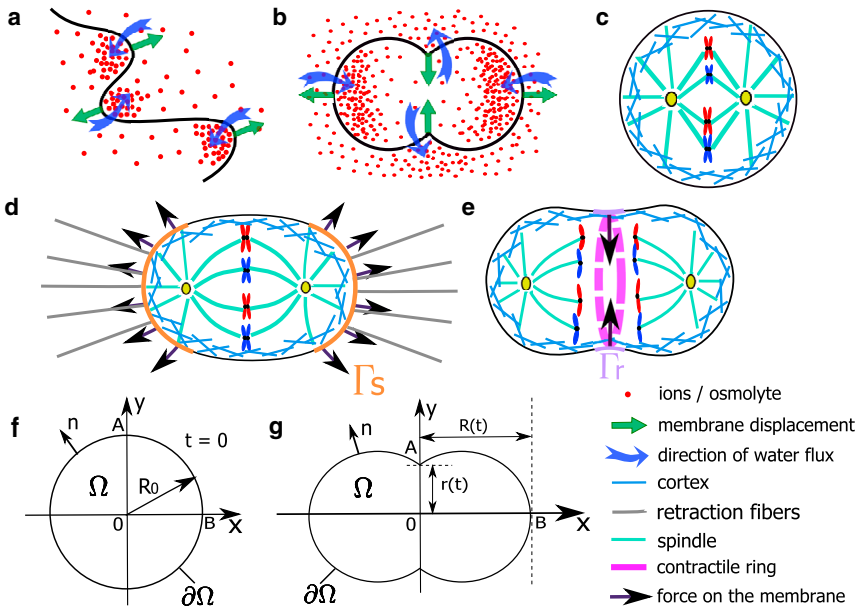

FIGURE 1 (*a*) Local osmolarity differences can drive water flow across the membrane. The water flux is normal to the surface in the direction of higher osmolarity. (*b*) A possible spatial arrangement of intracellular ionic distribution during cytokinesis. The cell shape is determined by the water flux across the membrane. The water flux is mostly determined by osmotic pressure differences, although mechanical forces on the cell boundary that influences hydrostatic pressure difference, also contribute. (*c*) Schematics of a spherical cell before cytokinesis occurs. The cell boundary is composed of a lipid bilayer and an actin cortex. (*d*) The mitotic spindle or retraction fibers provide(s) normal pushing forces on the cell boundary. Γ_s is the portion on the boundary where there could be a pushing force. (*e*) The contractile ring provides an inward normal force on the cell boundary. Γ_r is the portion of the boundary where there is a contractile force. (*f* and *g*) Schematics of the model and coordinate setup. The domain of the cell is denoted as Ω and the boundary is $\partial\Omega$. The value $\mathbf{n}$ is the unit norm vector on the boundary. *A* is the intersection of the cell boundary and the positive *y* axis; *B* is the intersection of the cell boundary and the positive *x* axis. $r(t) = |\mathbf{x}(A) - \mathbf{0}|$ and $R(t) = |\mathbf{x}(B) - \mathbf{0}|$, with $R(0) = r(0) = R_0$. To see this figure in color, go online.

furrow membrane (22). From our own experiments, a moderate depolymerization of the actin network does not affect the speed and cell shape during cytokinesis in HT1080 cells (see the Supporting Material). From modeling, we find that water flux can work together with the contractile ring to form the division furrow. This water-driven shape change is possible when water influx occurs at the two polar ends and efflux occurs at the cell midsection (see Fig. 1 *b* for an illustration). Such water flux distribution can be driven by a polarized distribution of intracellular ions (Fig. 1 *b*), which can arise from a spatial varying distribution of membrane ion channels and pumps. Experiments show that a type of chloride ion channel is enriched at the division furrow or at the cell poles, depending on the phase of cytokinesis. Blocking ion channels using drugs also can slow down or speed up cytokinesis, depending on the type of the targeted channels. These results suggest that cells potentially can employ multiple force-generating mechanisms available to ensure successful division.

To mathematically model water flux and actomyosin-driven cytokinesis, we employ a level-set moving boundary algorithm (23,24). We start with a cell where DNA replication is complete (Fig. 1 *c*) and model the process of cell elongation (Fig. 1 *d*) and ingression (Fig. 1 *e*). Possible forces from the mitotic spindle, retraction fibers (25) (Fig. 1 *d*), and the contractile ring (Fig. 1 *e*) are included in the model. We aim to understand, theoretically, how water permeation could facilitate cytokinesis with and without the contractile ring. We also experimentally manipulate water flux by exposing a dividing cell to hypotonic osmotic shock. We show that the observed kinematic changes can be explained by water flux alone, although in most cells both actomyosin contraction and water flow likely are coordinated together. This suggests that redundant mechanisms of cellular force generation increase robustness during essential cell shape changes.

MATERIALS AND METHODS

For simplicity, we consider a dividing cell in 2D as shown in Fig. 1, *f*–*g*. The symbol Ω represents the cell domain and $\partial\Omega$ is its boundary. The cell boundary is traced by the zero level set $\phi = 0$ and the intracellular space is given by $\phi < 0$ (23,24). The value $\mathbf{n}$ is the unit norm vector on the boundary pointing outwards. Pressure, velocity, and osmolyte concentration fields are solved for inside the cell, and the extracellular fields are assumed to be static and constant. *A* is the point on the boundary intersecting the *y* axis and *B* is the point on the boundary intersecting the *x* axis. Let $r(t) = |AO|$ and $R(t) = |BO|$, with $R(0) = r(0) = R_0$, where R_0 is the initial radius of the spherical cell at the beginning of cytokinesis. Fig. 1 *f* shows the initial state of the cell; Fig. 1 *g* shows the stage after ingression begins, but the septum between two daughter cells have not yet formed. Because we do not consider septum formation of the two daughter cells, in this work we only model the cell shape progression from Fig. 1 *f* to Fig. 1 *g*.

We consider force balance at the cell surface as a combination of tension *T* in the lipid bilayer and an active contractile stress from the cortex beneath the bilayer (Fig. 1 *c*). Because the lipid bilayer is a fluid and undergoes turnover from lipid-trafficking, we assume that *T* does not vary during cytokinesis. The actin cortex also undergoes fast turnover and exerts an active contractile stress σ_a tangential to the cell surface. This force balance problem at the cell surface for an active liquid cortex was considered in detail (26). Here we assume a constant cell surface tension, $\tau = T - \sigma_a h$, where *h* is the cortical thickness. This assumption excludes the case where spatially and temporally varying cortical tension may drive cytokinesis. Hence, this work focuses on water-flux-facilitated cytokinesis under uniform tension (see the Supporting Material for a discussion on the role of spatially varying tension on the cytosol flow field).

Within the model, we can also consider possible forces from the contractile ring and from the mitotic spindle or retraction fibers (Fig. 1, *d* and *e*). Let $q_s(\mathbf{x},t)$ be the outward force per unit area normal to the boundary of

the cell from the spindle pushing or retraction fibers pulling. The value q_s is only defined on Γ_s and is 0 for regions outside of Γ_s, where Γ_s is the portion on the boundary where pushing force exists. The contractile ring force, $q_r(\mathbf{x},t)$, is defined in a similar way. Considering all the forces on the cell surface, the force balance condition in the normal direction is

$$\tau(\mathbf{x})\kappa(\mathbf{x}) = \Delta p(\mathbf{x}) + q_s(\mathbf{x}) - q_r(\mathbf{x}), \quad (1)$$

where κ is the cell surface curvature. The value $\Delta p(\mathbf{x}) = p(\mathbf{x})|_{\partial\Omega^-} - p_0$ is the hydrostatic pressure difference across the membrane, where p_0 is the constant extracellular hydrostatic pressure.

The intracellular hydrostatic pressure comes from cytosol, the noncytoskeleton part of the cytoplasm. Hereafter we will use the term "fluid" to refer to the cytosol and use the term "network" to refer to the cytoskeleton network including actin, myosin, and microtubules. We model the intracellular fluid as a Stokes flow,

$$-\nabla p + \mu_f \nabla^2 \mathbf{V}_f + \mathbf{f} = 0, \quad (2)$$

where μ_f is the dynamic viscosity of the intracellular fluid. The value $\mathbf{f}$ is the effective body force due to the frictional drag between various network structures and the intracellular fluid. Prior work has shown that the cell network is porous (10); therefore, as the fluid flows, there is a drag force between the network phase and the fluid phase. The value $\mathbf{f}$ is proportional to the fluid velocity but points to the opposite direction of the flow, i.e., $\mathbf{f} = -\eta_c \mathbf{V}_f$, where η_c is the drag coefficient depending on the viscosity of the fluid and the density of the network. This viscous drag exerts an equal and opposite reaction force on the actin network phase, which also flows. Most of the actin flow occurs in the thin cell cortex during cytokinesis, and flows from the membrane toward the interior of the cell with mass turnover from actin polymerization and depolymerization. The net actin velocity along a typical stream line of the cytosol flow is approximately zero, and therefore should not influence the cytosol flow significantly. Moreover, during cell division when the cell is rounded up, the actin cytoskeleton is anchored to the substrate through adhesions and traction fibers. Therefore, any reaction force from the cytosol phase onto the network phase is ultimately transmitted to the substrate. We therefore do not consider the dynamics of the actin phase in this model (see the Supporting Material for a two-phase treatment).

The Laplace operator term in Eq. 2 is on the order of $1/{R_0}^2$, where the radius of the cell is $\sim$10 μm. The value η_c used here is $\sim 10^1 \sim 10^3$ pN$\cdot$s/μm^4, which gives realistic intracellular fluid velocities of $<$0.02 μm/s (see below). We thus have $\mu_f/{R_0}^2 << \eta_c$ and Eq. 2 can be simplified as

$$-\nabla p - \eta_c \mathbf{V}_f = 0. \quad (3)$$

Physically, this means that the fluid viscosity is negligible compared to the viscous drag between the fluid and the network. From Eq. 3 and the assumption that the drag coefficient η_c is a constant in space, the incompressibility condition $\nabla \cdot \mathbf{V}_f = 0$ is equivalent to $\nabla^2 p = 0$, which can be solved with the boundary condition in Eq. 1 (see the Supporting Material for more information). Once the pressure p is solved, $\mathbf{V}_f$ is obtained from Eq. 3.

The velocity of the cell membrane at each point $\mathbf{x} \in \partial\Omega$ can be decomposed into two components, one normal to the boundary and the other tangential to the boundary. The tangential component generates membrane flow within the lipid bilayer and does not contribute to the observed shape change. The normal component, on the other hand, advances the cell boundary during cytokinesis and is responsible for the cell shape change from Fig. 1 *f* to Fig. 1 *g*. Therefore, the normal velocity of the membrane, V_m, is a combination of boundary flux and intracellular fluid flow at the boundary (27), i.e.,

$$V_m = \mathbf{V}_f\big|_{\partial\Omega^-} \cdot \mathbf{n} - V_p, \quad (4)$$

where V_p is the velocity of water flux across the cell membrane. The value V_p is negative for water influx and positive for water efflux. It is clear that the cell shape and forces needed to generate the observed cell shape depends on V_p, which is often not discussed, or is assumed to be zero. Here we are interested in examining the effect of V_p on cell shape and mechanics. V_p is related to the local osmotic imbalance between inside and outside of the cell, and also any mechanical tension changes in the cell cortex:

$$V_p = \alpha_m(\Delta p - RT\Delta c), \quad (5)$$

where α_m is the permeation coefficient of the cell membrane, and Δp is determined by Eq. 1. $\Delta c = c\,|_{\partial\Omega^-} - c_0$, where c is the intracellular osmolyte concentration and c_0 is the extracellular concentration. To obtain shape changes, V_p must be nonuniform, i.e., there are regions on the cell surface where the flux may be large or positive whereas at other places the flux may be small or negative. We see that spatial variation in V_p can come about in multiple ways. From Eq. 1 the hydrostatic pressure difference can vary as a function of space. From variations in location of ion channels and pumps, Δc could also vary as a function of space. Finally, α_m, which is proportional to aquaporin concentration at the cell surface, could also vary spatially. To avoid complexity associated with spatially varying generators of water flux, we will first prescribe V_p as a function of space to illustrate how it can affect the cell shape. We then use an example to show how spatial variation of ion pumps can determine the water flux across the membrane. To do that, we need intracellular ionic dynamics for the model. Because we focus on the osmolarity of the cytoplasm, in the model the osmolytes are assumed to be electro-neutral.

The intracellular osmolyte concentration, c, is governed by the diffusion equation

$$\frac{\partial c}{\partial t} = \nabla \cdot \left(D\nabla c - c\mathbf{V}_f\right), \quad (6)$$

where D is the diffusion constant. The boundary condition for Eq. 6 is the osmolyte flux, $J_c = -D\nabla c + c\mathbf{V}_f$, across the cell boundary. In general, this flux is the sum of passive and active fluxes, and we take the convention that it is positive inwards. The passive flux is proportional to the concentration difference across the membrane, i.e., $J_{\text{passive}} = -\beta(c\,|_{\partial\Omega^-} - c_0)$, where β is a constant. The active osmolyte transport requires energy input, and can occur in either direction, depending on the type of the pump. In this model, we use $J^{\text{in}}_{\text{active}}$ ($J^{\text{out}}_{\text{active}}$) to represent the effective in-flux (out-flux) of osmolytes by all possible pumps, which depends on the extracellular (intracellular) concentration and the spatial distribution of pumps. We let $J^{\text{in}}_{\text{active}} = \gamma_{\text{in}}(\mathbf{x})c_0$, where γ_{in} is a spatial varying coefficient representing the distribution of pumps that can transport osmolytes into the cell. Similarly, $J^{\text{out}}_{\text{active}} = \gamma_{\text{out}}(\mathbf{x})c\,|_{\partial\Omega^-}$. The values $\gamma_{\text{in,out}}$ are nonuniformly distributed during cytokinesis. Energy consumption by the active pumps is implicitly contained in the $\gamma_{\text{in,out}}$. This spatial distribution could arise from spindle-based transport or direct positioning of membrane proteins by the contractile ring. The total flux can thus be expressed as

$$J_c = J_{\text{passive}} + J^{\text{in}}_{\text{active}} + J^{\text{out}}_{\text{active}}, \quad (7)$$

which is a boundary condition to Eq. 6.

The initial intracellular ion concentration is constant in space and is determined by the pressure balance: if the initial hydrostatic pressure difference across the cell membrane is Δp_0, i.e., $p|_{t=0} = p_0 + \Delta p_0$, then the initial intracellular ion concentration is $c|_{t=0} = c_0 + \Delta c_0$, where $\Delta c_0 = \Delta p_0/RT$.

The system of equations is solved using the level set-finite volume method. Details of the methods are given in the Supporting Material.

RESULTS

Shape of dividing cell

We first consider the situation in which the prescribed water flux is

$$V_p(x) = \left(\alpha_c - \frac{\alpha_c + \beta_c}{R(t)}|x|\right)v_0, \quad (8)$$

where α_c and β_c are 2D scalars and $v_0 = \alpha_m \Delta p_0$ is the velocity scale of the problem. Therefore, V_p is $\alpha_c v_0$ at $(0, \pm r)$ and $-\beta_c v_0$ at $(\pm R, 0)$. In general, we allow $\alpha_c = \alpha_{c0} T_\alpha(t)$ and $\beta_c = \beta_{c0} T_\beta(t)$ to vary with time. When $|\mathbf{V}_f \cdot \mathbf{n}| << |V_p|$, the cell surface velocity is close to V_p. Fig. 2 *a* shows V_m derived solely from V_p in Eq. 8. In this case, $-V_p$ closely approximates rates of change of the small and large radii, i.e., $dr/dt \sim -\alpha_c v_0$ and $dR/dt \sim \beta_c v_0$. We therefore use these two rate parameters to characterize the shape dynamics of the cell. Equation 8 gives the prototypical shape of a dividing cell as shown in Fig. 2 *b*. To preserve the overall cell volume, $\int_{\partial\Omega} V_p ds = 0$ is required. Fig. 2 *c* shows the profile of $\mathbf{V}_f$ at an early time given the water flux in Eq. 8. This $\mathbf{V}_f$ pushes the center of the cell near the division plane outwards. When $|\mathbf{V}_f \cdot \mathbf{n}|$ is comparable to $|V_p|$, the cell boundary velocity is also affected by $\mathbf{V}_f$. In this case, dr/dt and dR/dt are sums of V_p and $\mathbf{V}_f$.

Experiments show that r and R during cytokinesis are approximately linear functions of time, suggesting that dr/dt and dR/dt are approximately constants. Using parameters in Table S1, which gives $|\mathbf{V}_f \cdot \mathbf{n}| << |V_p|$, the cell shape change over time is given in Fig. 2 *e* and the profile of V_m at time $t = 200$ s is shown in Fig. 2 *f*. This shows the achievement of the ideal shape-phenotype, in which the change in $r(t)$ and $R(t)$ from simulation matches experimental measurement (Fig. 2 *d*).

Effects of the contractile force

However, when the drag between the network and the fluid, η_c, is reduced by approximately two orders of magnitude,

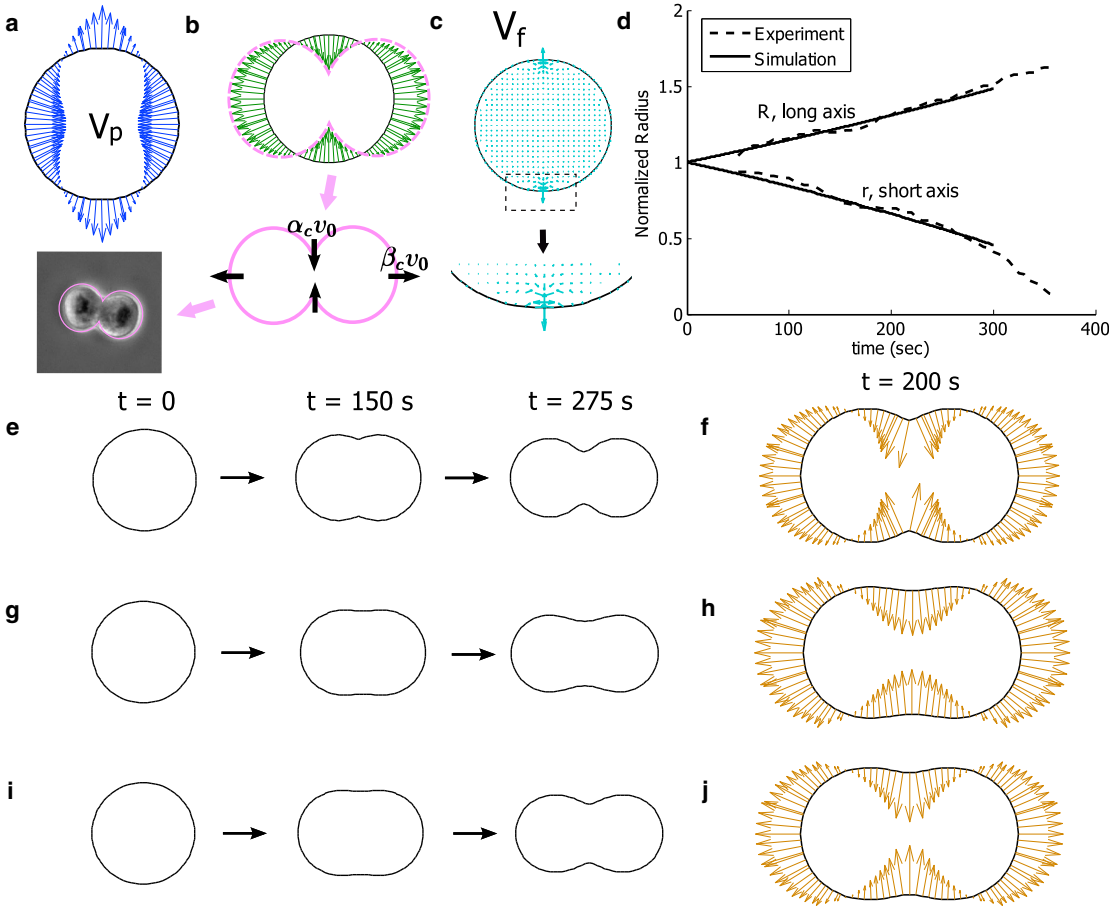

FIGURE 2 (*a*) An example of spatially varying water flux. V_p is pointing outwards at points close to the division plane and inwards at the poles. (*b*) In this case, cell boundary velocity at point *A* is $\alpha_c v_0$ pointing inwards, and the boundary velocity at point *B* is $\beta_c v_0$ pointing outwards. The resulting cell boundary from this V_p gives the characteristic shape observed during cytokinesis that matches the experimental shape. (*c*) A sample profile of the computed intracellular fluid velocity, $\mathbf{V}_f$. This fluid field pushes the cell membrane outwards near the division site. The final cell boundary velocity is a combination of V_p and $\mathbf{V}_f$ that work in opposite directions. (*d*) Normalized long (R) and short (r) axes of a dividing cell with time. The normalization factor is the cell radius at the initial stage. The simulation is based on the parameters listed in the Supporting Material. (*e*, *g*, and *i*) Shapes of the dividing cell at $t = 0$, $t = 150$ s, and $t = 275$ s with three different simulation conditions. (*f*, *h*, and *j*) The cell boundary velocity at $t = 200$ s corresponding to the conditions used in (*e*), (*g*), and (*i*), respectively. (*e* and *f*) $\eta_c = 5 \times 10^3$ pN • s/μm^4; (*g* and *h*) $\eta_c = 25$ pN • s/μm^4; (*i* and *j*) $\eta_c = 25$ pN • s/μm^4 with contractile force, q_r, from the contractile ring. To see this figure in color, go online.

$|\mathbf{V}_f|$ increases and becomes comparable with $|V_p|$. In this case, the shape of the cell during division is more rounded at the center of the mother cell (Fig. 2 *g*). This can be seen in Fig. 2 *h* where the V_m becomes smooth at the middle of the cell due to the opposing contribution from $\mathbf{V}_f$. One possible solution is to adjust the profile of V_p to compensate for the effect of $\mathbf{V}_f$. Alternatively, we find that forces from the contractile ring also influence the cell shape. Let Γ_r be the region on the cell boundary where $|x| < R_0/10$, modeling the location of the contractile ring. Within Γ_r, we let q_r be an increasing function of time, defined as $q_r = Q_{r0}(t - T_R)H(t - T_R)$, where Q_{r0} is a constant and T_R is the time after which the contractile ring begins to exert force. $H(t)$ is a step function that is 1 for $t > 0$ and 0 otherwise. Fig. 2 *i* shows that the presence of the contractile force helps to develop the typical cell shape seen during cytokinesis because it increases the velocity of V_m at the center of the cell (Fig. 2 *j*).

We also find that the contractile force should be regulated in time. The value $q_r(t)$ in Fig. 2 *i* (see also table of parameters in the Supporting Material) reaches a maximum contractile stress, 450 Pa, at $t = T_0$, corresponding to a force ~10 nN based on the geometry of the cell. This force is on the same order as the contractile force estimated from modeling the contractile ring (28). An earlier activation of the contractile force (smaller T_R) or a larger Q_{r0} does lead to a shorter r at $t = T_0$ (see the Supporting Material). We can also incorporate forces from the spindle/retraction fibers, and spatially varying cell surface tension and aquaporins, but a global coordination of these forces is needed to generate the observed cell shape during cytokinesis.

Hypotonic shock during cytokinesis

Water flux across the cell membrane is influenced by the extracellular osmolarity. To further investigate the role of water flux during cytokinesis, we performed osmotic shock experiments on HT1080 cells. A hypotonic shock during cytokinesis immediately increases the water influx and thus the cell radii $r(t)$ and $R(t)$ (Fig. 3 *a*). The increase of R was expected, but dR/dt increased as well after the shock (Fig. 3 *b*). Moreover, the increase in r due to the osmotic shock was only temporal, followed by an increased $|dR/dt|$ (Fig. 3 *b*). The fast decrease of r after the shock ensured the completion of the cytokinesis within the same time frame as without osmotic shock (compare the *dashed lines* in Figs. 3 *b* and 2 *d*), suggesting that there is a compensatory control mechanism that is robust to external perturbations.

The speedup of $|dr/dt|$ may come from increases in the contractile force from the cytokinetic ring. Here we find that water flux can also generate a similar compensatory effect. To obtain a sudden increase of water influx upon the shock, T_α and T_β must be functions of time. For example, T_α and T_β can be adjusted as shown in Fig. 3 *c*. The jump implies that there needs to be a sudden water influx upon shock and its magnitude is related to the strength of the shock. T_α and T_β do not typically follow the same pattern, because

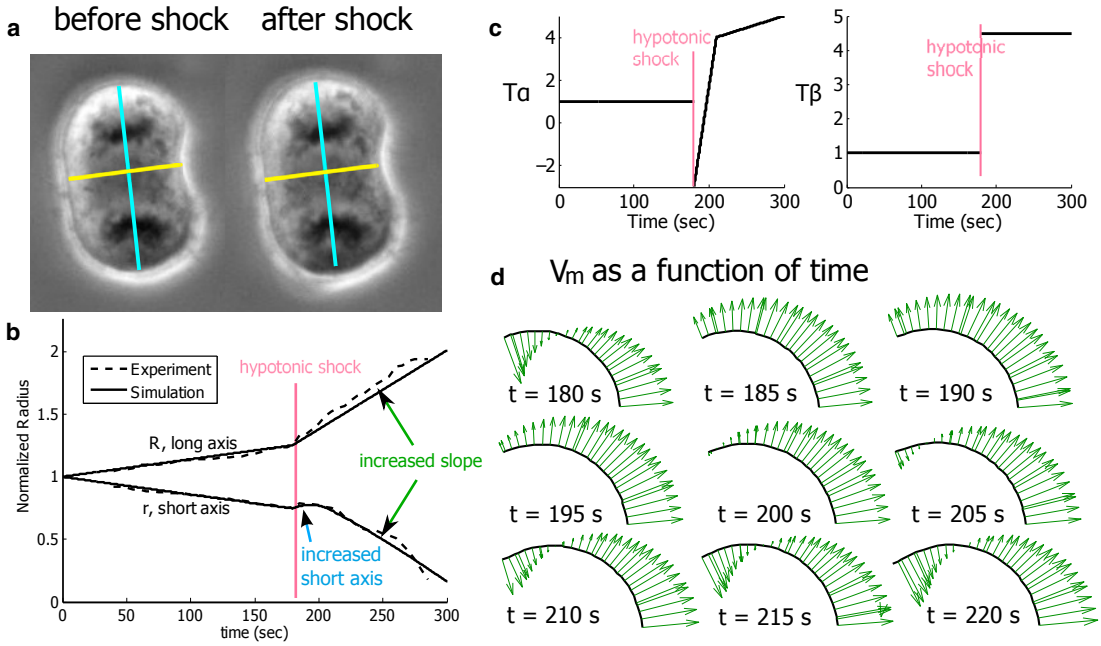

FIGURE 3 Cytokinesis with hypotonic shock. (*a*) Phenotype of a dividing cell before and after a hypotonic shock. The time gap between the two frames was 5 s. The two measuring bars (one for the long axis and one for the short axis) show the increased cell size after the hypotonic shock. (*b*) Experimental and simulation results for cytokinesis with a hypotonic shock. The vertical line indicate the start of the shock. (*c*) The profiles of $T_\alpha(t)$ and $T_\beta(t)$ used in the simulation in (*b*). (*d*) The profiles of V_m at different time points before and after the shock. V_p adjustment must arise either from actions of ion pumps or changes in the contractile force. To see this figure in color, go online.

different ion channels/pumps are operating at different regions, and the ion pump may redistribute in response to a shock. The sample profiles shown in Fig. 3 *c* suggest that pumps transporting ions outwards may soon accumulate at the middle of the cell upon shock to facilitate the completion of cytokinesis. A similar recovery of T_α is also predicted by a model of cell volume regulation (29). Before the shock, the ingression velocity induced by the water flux is the same as before (Fig. 3 *d*, $t = 180$ s); immediately after the shock, this velocity points outwards everywhere (Fig. 3 *d*, $t = 185$ s). The adjusted water flux with hypotonic shock captures the feature of the cell shape change (Fig. 3 *b*). Alternatively, changes in water flux could also result from time-dependent changes in the contractile force q_r. It is known that the actomyosin ring has mechanosensitive properties (30), and because q_r directly influences hydrostatic pressure difference in Eq. 1, it would also alter V_p.

Ion dynamics

We have shown that a cell with prescribed membrane water flux is able to generate the characteristic cell shape during cytokinesis. In our proposed mechanism, water flux and thus the ion distribution play a role in facilitating cytokinesis. Next, we will illustrate how ions can distribute to generate the type of water flux. One possibility is that during cytokinesis, there is more active ion efflux at the middle of the cell and more influx at the two polar ends. We find that if γ_{in} depends linearly on the cell curvature $\gamma_{in} = \gamma^0{}_{in}\,(c_1 + c_2\kappa(t))$ and $\gamma_{out} = \gamma^0{}_{out}[1-|x|/R(t)]$, where $\gamma^0{}_{in}$, $\gamma^0{}_{out}$, and $c_{1,2}$ are constants, then V_p (Eq. 5) has the same profile as Eq. 8. This type of ion channel spatial profile can come from cytoskeleton-mediated (either microtubule or actin) membrane vesicle trafficking. For the parameters listed in the Supporting Material, $\gamma_{in/out}$ gives a maximum ion flux on the order of $10^8\ \mu m^{-2}\ s^{-1}$. From known properties of various channels, this flux requires $\sim 10^3$ passive channels and $\sim 10^5$ active pumps per μm^2 (12). The computed radius over time is shown in Fig. 4 *a*; the reasonable match between the experiments and the simulation indicates that $\gamma_{in/out}$ is a possible distribution of ion channels and pumps facilitating the shape change during cytokinesis. Fig. 4 *b* shows the spatial distributions of the intracellular hydrostatic pressure and osmotic pressure at $t = 150$ s. Each has been subtracted by its corresponding extracellular pressure for clear visualization. Both pressures are high at the two polar ends and low in the middle of the dividing cell, and the maximum intracellular pressure difference is $\sim$200 Pa. This difference is in the same range of the rounding pressure in mitotic cells generated by actomyosin (31). It suggests that ion dynamics and actomyosin contraction may work cooperatively during cell division. The spatial hydrostatic pressure variation generates an intracellular fluid velocity shown in Fig. 4 *b*; this velocity is high and points outwards at the middle of the cell (also see Fig. 2 *c*). At $t = 275$ s, the shape of the cell is different from that at $t = 150$ s, but the spatial patterns of the hydrostatic and osmotic pressures are similar. With the given ion pump distribution, the two pressure patterns are maintained over time.

To examine spatial distribution of ion channels during cell division, we fixed and stained HT1080 cells for a chloride channel CLIC1 at early and late stages of cytokinesis (Fig. 4, *d* and *e*, *upper panels*; see the Supporting Material for more information). During the elongation phase of cytokinesis, CLIC1 was more concentrated at the division furrow (Fig. 4 *d*, *lower panel*). At a late stage of cytokinesis, CLIC1 was no longer concentrated at the division furrow and moved to the middle of the two daughter cells (Fig. 4 *e*, *lower panel*), suggesting that there are both temporal and spatial regulation of the CLIC1 channel during cytokinesis. To further examine the role of ion channels in cytokinesis, we blocked several types of channels using drugs (EIPA, DCPIB, and NPPB) and found that when multiple types of ion channels are blocked simultaneously, the total cytokinesis time was increased by 58% (Fig. 4 *f*). The slowdown was more prominent during the elongation stage ($p < 0.0001$) and less significant during the contraction stage ($p < 0.01$; see the Supporting Material for more information). Interestingly, when these drugs were applied individually, cytokinesis was either not affected or even increased in speed (NPPB, for example). This suggests that cells may utilize different ion channels based on their availability. Blocking one type of ion channel may readjust the ion fluxes across the membrane and lead to a faster cytokinesis. But when multiple channels are blocked at the same time, the final effect is not simply a linear superposition from the blockage of each individual channel. There is a complex coordination mechanism that maintains robustness. Collectively, the above results suggest that there exists a coordinated and carefully regulated system involving both contraction and ion permeation during cytokinesis.

In reality, fluxes of Na^+, K^+, and Cl^-, along with possible Ca^{2+} and HCO^{3-} fluxes, all contribute to the final total flux. Na^+/K^+ exchanger is one of the most important ion pumps in regulating cell ionic content (32), but cotransporters such as the NaKCl cotransporter are also involved (33). The exact contributions of each type of ion, and the associated electric fields are complex (12). In addition, the ion gradients will lead to small membrane voltage gradients during cytokinesis.

Impermeable cell

In the case when $V_p = 0$, we find that the cell cannot form the division furrow with contractile force q_r and/or pushing force q_s, when the membrane tension, τ, is kept constant (see the Supporting Material for detailed information). This is because the hydrostatic pressure field formed from the contractile force is not compatible with the relationship between curvature and cell surface tension near

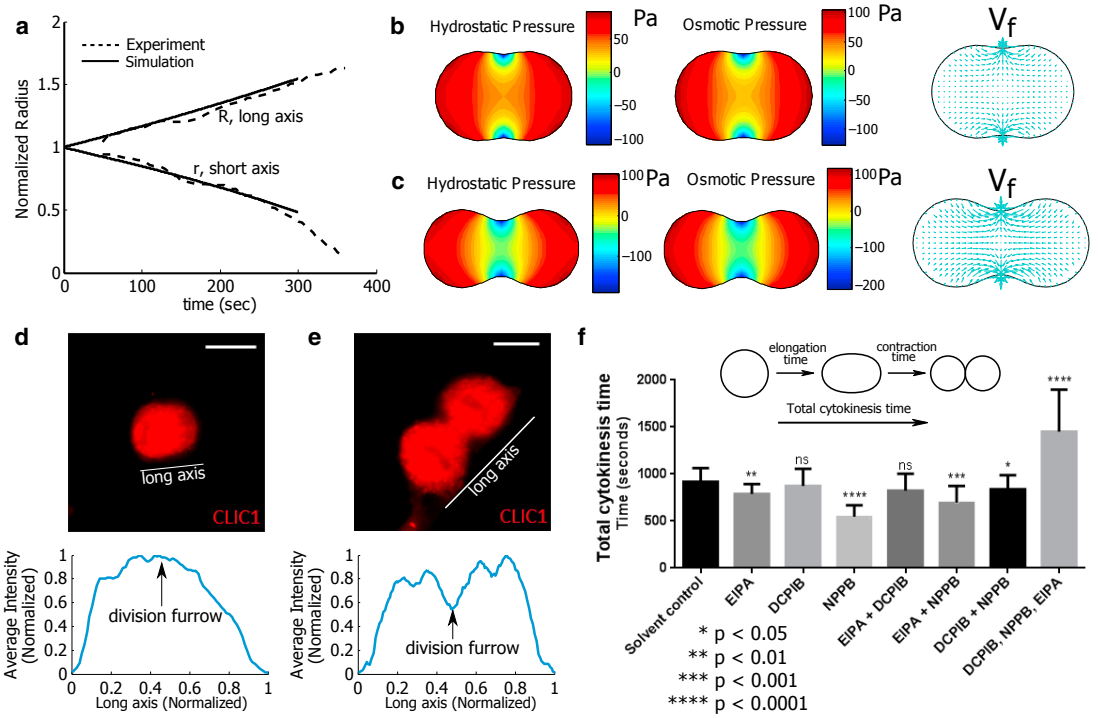

FIGURE 4 Cytokinesis with ion dynamics. (*a*) Normalized long (R) and short (r) axes of a dividing cell with time. Numerical simulation with ion dynamics is compared against experimental data. (*b* and *c*) Spatial distributions of the intracellular hydrostatic pressure and osmotic pressure at $t = 150$ s (*b*) and $t = 275$ s (*c*). Each has been subtracted by its corresponding extracellular pressure. Note that the osmotic pressure gradient across the cell is ~200 Pa. This corresponds to a concentration difference of ~0.5 mM from the cell pole to the division furrow. The corresponding intracellular fluid velocity profiles are also shown. (*d*) (*Upper panel*) Fixed and stained image of chloride channel CLIC1 in HT1080 at an early stage of cytokinesis. (*Lower panel*) CLIC1 intensity along the long axis of the cell. (*e*) (*Upper panel*) Fixed and stained image of CLIC1 in HT1080 at a late stage of cytokinesis. (*Lower panel*) CLIC1 intensity along the long axis. (*d* and *e*) Scale bars, 20 μm. (*f*) Effects of different ion channel blockers on the total HT1080 cytokinesis time (see the Supporting Material for more details). DCPIB is a specific blocker of the volume-sensitive anion channel and $I_{Cl,swell}$. NPPB inhibits Ca^{2+}-sensitive Cl^- currents. EIPA is an inhibitor of the Na^+/H^+ exchanger. Solvent control: ethanol and methanol in DMEM+10% FBS, $n = 31$, mean ± SD = 919 ± 144 s; EIPA: $n = 11$, mean ± SD = 787 ± 104 s; DCPIB: $n = 29$, mean ± SD = 874 ± 183 s; NPPB: $n = 9$, mean ± SD = 544 ± 124 s; EIPA + DCPIB: $n = 5$, mean ± SD = 824 ± 181 s; EIPA + NPPB: $n = 9$, mean ± SD = 693 ± 179 s; DCPIB + NPPB: $n = 31$, mean ± SD = 837 ± 152 s; and DCPIB, NPPB, EIPA: $n = 6$, mean ± SD = 1450 ± 448 s. All of the drugs are 100 μM in DMEM. (*Inset*) The total cytokinesis time is defined as the combined time of the elongation stage and contraction stage. To see this figure in color, go online.

the poles (Eq. 1). Therefore, to form the furrow when the cell is impermeable, the cell must actively readjust cortical tension τ via a signaling mechanism. This type of cortical tension change and flow that drives cytokinesis has been proposed and discussed (20,34,35). In the case where the membrane is permeable, τ can remain constant while forming the division furrow, as has been demonstrated in this work.

Role of external fluid field

Here we discuss the effect of external fluid field on cytokinesis. In the model we have assumed that when the cell is in 2D culture, the external fluid pressure field is static and constant. The assumption holds when $|\mathbf{V}_f \cdot \mathbf{n}| << |V_p|$ because, in this case, $V_m = -V_p$ and the external fluid remains static with zero velocity. In the extreme case of $|\mathbf{V}_f \cdot \mathbf{n}| >> |V_p|$, we estimate the external fluid pressure variation as follows. Let us consider the initial stage of cytokinesis when the cell is essentially spherical. The fluid flux is outward at the middle of the sphere and inward at the poles, which is equivalent to a boundary condition for the normal component of the external flow: $\mathbf{V}_{\text{ext}}|_{\partial\Omega^+} \cdot \mathbf{n} = -v_r \cos(2\theta)$, where θ is the angle with respect to the x axis and v_r is the maximum external fluid velocity on the cell boundary. The extracellular pressure distribution in this case is $p|_{\partial\Omega^+} = p_0 - 4\mu v_r \cos(2\theta)/R_0$, where p_0 is the far-field pressure and μ is the dynamic viscosity of the external fluid. For $R_0 = 10$ μm and velocity of the order 1 μm/min, the pressure variation is on the order of 10^{-5} Pa around the cell, which is negligible when compared with the pressure difference across the cell membrane. The external fluid field can thus be safely neglected.

When the cell is not in 2D culture where there is infinite extracellular space, the external pressure field may vary around the cell boundary. In this case, we can rewrite Eq. 1 as

$$p(\mathbf{x})|_{\partial\Omega^-} = \tau(\mathbf{x})\kappa(\mathbf{x}) + q_r(\mathbf{x}) - q_s(\mathbf{x}) + p_0(\mathbf{x})|_{\partial\Omega^+}. \quad (9)$$

The terms $q_r(\mathbf{x}) - q_s(\mathbf{x}) + p_0(\mathbf{x})\,|_{\partial\Omega^+}$ work together as additional forces on the cell boundary. The value p_0 may add or subtract from $q_{s,r}$, depending on the distribution of $p_0\,|_{\partial\Omega^+}$. We would thus expect a similar contribution from $p_0\,|_{\partial\Omega^+}$ on the force balance of the cell membrane as $q_{s,r}$. Meanwhile, Eq. 5 should be rewritten as

$$V_p = \alpha_m(p\,|_{\partial\Omega^-} - p_0\,|_{\partial\Omega^+} - RT\Delta c). \tag{10}$$

Substituting Eq. 9 into Eq. 10 yields

$$V_p = \alpha_m(\tau\kappa - q_s + q_r - RT\Delta c), \tag{11}$$

which remains the same as we neglect the effect of spatially varying p_0. Hence, nonuniform $p_0(\mathbf{x})$ affects the cell shape similar to $q_{s,r}$, but does not alter the water flux through the cell membrane.

DISCUSSION

In this article, our modeling work suggests that water permeation, in principle, can contribute to cell shape changes and facilitate cytokinesis. Depending on the magnitude of the intracellular fluid flow, the cell shape change can occur with or without the contribution from the contractile ring. The intracellular fluid velocity comes from the intracellular hydrostatic pressure gradient. This gradient can be generated in several ways, and in this model, it is caused by nonuniform ion channel distribution and osmolyte fluxes from the cell boundary. We found that one can achieve the necessary cell shape changes if the ion flux depends on the cell boundary curvature. The steepness of the pressure gradient is also related to the cortical tension (Eq. 1), and a larger pressure gradient is needed to balance higher cortical tension. Intracellular hydrostatic pressure differences are typically present when the cytoplasm has complex structure so that the pressure cannot balance immediately. Cells with compartmentalized intracellular structure also have nonuniform hydrostatic pressure, the difference of which can be on the order of 1 kPa (36).

In our model, in addition to the hydrostatic pressure gradient that varies in space and time, the magnitude of the intracellular velocity is also affected by the viscous drag between the fluid and the network. Here we treat the network as a poroelastic material (10). When $\eta_c = 25$ pN $\cdot$ s/μm^4, the maximum intracellular fluid velocity is $\sim$0.02 μm/s at the late stage of cytokinesis. For larger η_c, $|\mathbf{V}_f|$ is even smaller. The intracellular fluid velocity varies under different conditions and geometries. Previous measurements have shown that in a rapid moving cell in 2D, the average intracellular fluid velocity can be higher than what we have predicted in our model, $\sim$0.11 μm/s (9). For cells confined in 1D narrow channels, the fluid velocity may reach $\sim$0.2 μm/s (4). Therefore, the flow fields needed to generate the observed cell shape are small, and are consistent with known intracellular flow fields outside of the division context.

We find that spatially varying boundary water flux can arise from spatially varying distributions of ion channels and pumps. This type of membrane channel arrangement can arise from active transport of vesicles in the cytoplasm, or by direct recruitment by the contractile ring. Of course, the cytoskeleton itself has complex behavior. The main focus of this article is on the potential contribution of membrane water flux to cytokinesis. It is clear that the physical processes that lead to cytokinesis may be complex, and can involve the contractile ring, spatially varying cortical tension, and forces at the cell poles. The cell uses these multiple mechanisms to ensure robustness and timing of cell division. The global signaling mechanisms that control these mechanical elements require more careful examination. More generally, water flux and hydrodynamics are likely to play important roles in many aspects of cell shape and cell movement, both in single cells as well as tissue and organs. Beyond biological systems, directed water flow can be used as a means of mechanical actuation and, to our knowledge, novel method of force generation.

SUPPORTING MATERIAL

Supporting Materials and Methods, eight figures, and one table are available at http://www.biophysj.org/biophysj/supplemental/S0006-3495(17)31069-X.

AUTHOR CONTRIBUTIONS

Y.L., D.W., and S.X.S. conceived and designed the experiment. Y.L. and S.X.S. designed the model. L.H., N.A.P.G., and J.G. performed the experiments. C.W. supplied the modeling code. Y.L., L.H., and S.X.S. wrote the article.

ACKNOWLEDGMENTS

This work has been supported by National Institutes of Health (NIH) grants R01GM114675 and U54CA210172.

REFERENCES

1. Koeppen, B. M., and B. A. Stanton. 2013. Renal Physiology, 5th Ed. Mosby Physiology Monograph Series. Elsevier, Amsterdam, Netherlands.
2. Hoffmann, E. K., I. H. Lambert, and S. F. Pedersen. 2009. Physiology of cell volume regulation in vertebrates. *Physiol. Rev.* 89:193–277.
3. Qiu, Z., A. E. Dubin, …, A. Patapoutian. 2014. SWELL1, a plasma membrane protein, is an essential component of volume-regulated anion channel. *Cell.* 157:447–458.
4. Stroka, K. M., H. Jiang, …, K. Konstantopoulos. 2014. Water permeation drives tumor cell migration in confined microenvironments. *Cell.* 157:611–623.
5. Katchalsky, A. K., and P. F. Curran. 1965. Nonequilibrium Thermodynamics in Biophysics. Harvard University Press, Cambridge, MA.

6. Charras, G., and E. Paluch. 2008. Blebs lead the way: how to migrate without lamellipodia. *Nat. Rev. Mol. Cell Biol.* 9:730–736.
7. Tinevez, J. Y., U. Schulze, …, E. Paluch. 2009. Role of cortical tension in bleb growth. *Proc. Natl. Acad. Sci. USA.* 106:18581–18586.
8. Charras, G. T., T. J. Mitchison, and L. Mahadevan. 2009. Animal cell hydraulics. *J. Cell Sci.* 122:3233–3241.
9. Keren, K., P. T. Yam, …, J. A. Theriot. 2009. Intracellular fluid flow in rapidly moving cells. *Nat. Cell Biol.* 11:1219–1224.
10. Moeendarbary, E., L. Valon, …, G. T. Charras. 2013. The cytoplasm of living cells behaves as a poroelastic material. *Nat. Mater.* 12:253–261.
11. Strychalski, W., and R. D. Guy. 2016. Intracellular pressure dynamics in blebbing cells. *Biophys. J.* 110:1168–1179.
12. Li, Y., Y. Mori, and S. X. Sun. 2015. Flow-driven cell migration under external electric fields. *Phys. Rev. Lett.* 115:268101.
13. Panopoulos, A., M. Howell, …, R. L. Margolis. 2011. Glioblastoma motility occurs in the absence of actin polymer. *Mol. Biol. Cell.* 22:2212–2220.
14. Papadopoulos, M. C., S. Saadoun, and A. S. Verkman. 2008. Aquaporins and cell migration. *Pflugers Arch.* 456:693–700.
15. Kim, D. H., B. Li, …, S. X. Sun. 2015. Volume regulation and shape bifurcation in the cell nucleus. *J. Cell Sci.* 128:3375–3385.
16. Robinson, D. N., and J. A. Spudich. 2004. Mechanics and regulation of cytokinesis. *Curr. Opin. Cell Biol.* 16:182–188.
17. Scholey, J. M., I. Brust-Mascher, and A. Mogilner. 2003. Cell division. *Nature.* 422:746–752.
18. Straight, A. F., A. Cheung, …, T. J. Mitchison. 2003. Dissecting temporal and spatial control of cytokinesis with a myosin II inhibitor. *Science.* 299:1743–1747.
19. Guha, M., M. Zhou, and Y. L. Wang. 2005. Cortical actin turnover during cytokinesis requires myosin II. *Curr. Biol.* 15:732–736.
20. Gerisch, G., and I. Weber. 2000. Cytokinesis without myosin II. *Curr. Opin. Cell Biol.* 12:126–132.
21. Shimizu, Y., Y. Kushida, …, O. Numata. 2013. Formation and ingression of division furrow can progress under the inhibitory condition of actin polymerization in ciliate *Tetrahymena pyriformis*. *Zoolog. Sci.* 30:1044–1049.
22. Straight, A. F., and C. M. Field. 2000. Microtubules, membranes and cytokinesis. *Curr. Biol.* 10:R760–R770.
23. Sethian, J. A. 1996. Theory, algorithms, and applications of level set methods for propagating interfaces. *Acta Numer.* 5:309–395.
24. Wolgemuth, C. W., and M. Zajac. 2010. The moving boundary node method: a level set-based, finite volume algorithm with applications to cell motility. *J. Comput. Phys.* 229:7287–7308.
25. Cramer, L. P., and T. J. Mitchison. 1997. Investigation of the mechanism of retraction of the cell margin and rearward flow of nodules during mitotic cell rounding. *Mol. Biol. Cell.* 8:109–119.
26. Tao, J., and S. X. Sun. 2015. Active biochemical regulation of cell volume and a simple model of cell tension response. *Biophys. J.* 109:1541–1550.
27. Kim, Y., and C. S. Peskin. 2006. 2-D parachute simulation by the immersed boundary method. *SIAM J. Sci. Comput.* 28:2294–2312.
28. Mendes Pinto, I., B. Rubinstein, and R. Li. 2013. Force to divide: structural and mechanical requirements for actomyosin ring contraction. *Biophys. J.* 105:547–554.
29. Jiang, H., and S. X. Sun. 2013. Cellular pressure and volume regulation and implications for cell mechanics. *Biophys. J.* 105:609–619.
30. Ren, Y., J. C. Effler, …, D. N. Robinson. 2009. Mechanosensing through cooperative interactions between myosin II and the actin crosslinker cortexillin I. *Curr. Biol.* 19:1421–1428.
31. Stewart, M. P., J. Helenius, …, A. A. Hyman. 2011. Hydrostatic pressure and the actomyosin cortex drive mitotic cell rounding. *Nature.* 469:226–230.
32. Armstrong, C. M. 2003. The Na/K pump, Cl ion, and osmotic stabilization of cells. *Proc. Natl. Acad. Sci. USA.* 100:6257–6262.
33. Russell, J. M. 2000. Sodium-potassium-chloride cotransport. *Physiol. Rev.* 80:211–276.
34. Bray, D., and J. G. White. 1988. Cortical flow in animal cells. *Science.* 239:883–888.
35. Turlier, H., B. Audoly, …, J.-F. Joanny. 2014. Furrow constriction in animal cell cytokinesis. *Biophys. J.* 106:114–123.
36. Petrie, R. J., H. Koo, and K. M. Yamada. 2014. Generation of compartmentalized pressure by a nuclear piston governs cell motility in a 3D matrix. *Science.* 345:1062–1065.